Environmental Engineering and Management Journal

May 2021, Vol. 5, No. 5, 687-700
http://www.eemj.icpm.tuiasi.ro/; http://www.eemj.eu

"Gheorghe Asachi" Technical University of Iasi, Romania

PURE SODALITE SYNTHESIS, CHARACTERIZATION AND APPLICATION FOR HEAVY METAL IONS REMOVAL FROM AQUEOUS SOLUTIONS

Seyedeh Mahsa Kamyab[1], Soroush Modabberi[1]*, Craig Denver Williams[2], Alireza Badiei[3]

[1]School of Geology, College of Science, University of Tehran, Tehran, Iran
[2]School of Applied Sciences, University of Wolverhampton, Wolverhampton, England
[3]School of Chemistry, College of Science, University of Tehran, Tehran, Iran

Abstract

Pure sodalites were successfully synthesized from kaolinite taking the advantages of alkaline fusion technique. The synthesized sodalites were then characterized via XRD, SEM/EDX, and FTIR methods. The efficiency of these sodalites for treatment of Cu^{2+}, Zn^{2+} and Ni^{2+} ions in aqueous solutions was also scrutinized through batch adsorption experiments. Subsequently, the concentrations of Cu^{2+}, Zn^{2+}, and Ni^{2+} ions in final leachates were detected by ICP-OES analysis. Furthermore, the results proved that adsorption data fitted very well to Freundlich isotherm model assuming that the metal ions removal can be applied to multilayer adsorption. Moreover, the kinetics of the adsorption followed the pseudo-second-order model suggesting that the rate of adsorption process may be controlled by the chemical sorption. In brief, the synthesized sodalites excellent performance for heavy metal ions removal from aqueous solutions can shed light on their remarkable potential in purification applications. Additionally, considering high cost of the natural sodalite, synthesis of sodalites with homogeneous porous structure that can be used as great adsorbents would be profitable for environmental purposes.

Key words: adsorption, heavy metal ion, pure zeolitic phase, sodalite, synthesis

Received: February, 2020; Revised final: July, 2020; Accepted: October, 2020; Published in final edited form: May, 2021

1. Introduction

Heavy metal ions usually release into the environment as a result of industrial activities such as metallic, minelaying, inorganic chemical and storage battery manufacturing industries (Barakat, 2011; Huang et al., 2018; Blázquez et al., 2018). As a consequence, humans are exposed to these metal ions through water, air, food, or industrial settings (Anyanwu et al., 2018). Therefore, heavy metal ions pollution is currently of great concern due to their harmful impacts on humans health. On this issue, high intake of copper(II) ion causes liver damage, and then hepatocyte death (Llanos and Mercer, 2002). Consequently, damaged hepatocytes lead to neurotoxicity (Taylor et al., 2020). High exposure to zinc(II) ion results in depression, lethargy, neurological signs and increased thirst (Babel and Kurniawan, 2003; Khan and Wahab, 2007). Exposure to high concentration of nickel(II) ion brings on heart and liver damages, skin irritation and dermatitis (Denkhause and Salnikov, 2002).

Several methods are recently employed to remove the heavy metal ions from the environment. Among them, adsorption and ion exchange are effective techniques for such cases, since they are relatively cheap in operational costs, and flexible to switch to different applications (Salih, 2017; Thakur and Parmar, 2013).

Preparation of adsorbents with specific sorption properties is recently an interesting subject of research. In this context, Godiya et al. (2020) prepared

* Author to whom all correspondence should be addressed: e-mail: modabberi@ut.ac.ir; Phone: +98-9122145463; Fax: +98-2166491623

highly porous egg white/polyethyleneimine hydrogel for Cu^{2+}, Pb^{2+} and Cd^{2+} ions removal from aqueous solution. Godiya et al. (2019a) produced a silk fibroin/ polyethyleneimine composite hydrogel for Cu^{2+}, Pb^{2+}, Cd^{2+}, Zn^{2+}, Ni^{2+}, and Ag^{2+} ions remediation from aqueous solutions. Godiya et al. (2019b) applied a bio-based bilateral hydrogel containing carboxymethyl cellulose and polyacrylamide for Cu^{2+}, Pb^{2+} and Cd^{2+} ions removal from wastewater. Godiya et al. (2019c) fabricated a natural and highly efficient sodium alginate polyethyleneimine composite hydrogel for heavy metal ions removal from wastewater.

In addition, zeolites, as naturally occurring minerals, are currently made for certain industrial and environmental uses (Robson, 1998). Since, they have advantages over other ion exchangers, relying on their low-cost, and ion selectivity, generated by their rigid porous structures (Colella, 2005; Moshoeshoe et al., 2017). Therefore, zeolites can be suitable substitute for current costly manufactured sorbents used for heavy metal ions removal from aqueous solutions. In light of this, the present research was aimed to synthesis of pure zeolites and examine their usage in environmental applications. Accordingly, the fusion technique was applied as synthesis method due to its effectiveness for hydrothermal conditions enhancement to dissolve aluminosilicates and synthesis of zeolites (Ríos et al., 2009). Further, monometallic solutions containing Cu^{2+}, Zn^{2+} and Ni^{2+} ions were prepared to evaluate the synthesized zeolites removal efficiency.

2. Material and methods

2.1. Materials

2.1.1. Raw material and reagents

The kaolinite raw material, was obtained from Iran China Clay company which extracts kaolin from Zonouz kaolin Mine located at the East Azerbaijan province, 20 km northeast of Marand city, Iran. Sodium hydroxide, NaOH, (Purity: 98%; Merck, Index-No. 011-002-00-6) as well as Aluminum Chloride, $AlCl_3.6H_2O$, (extra pure; Merck EG-Nr./EC-No.201-705-8), were applied for synthesis process. Metallic salts of Copper (II) Chloride Dihydrate ($CuCl_2.2H_2O$), (Purity, 99+%; Sigma Aldrich Co., CAS Number: 10125-13-0); Zinc Acetate $(CH_3.COO)_2$ $Zn.2H_2O$), (Purity, 99.5%; BDH Chemical Ltd Poole England); and Nickel (II) Chloride Hexahydrate ($NiCl_2.6H_2O$), (Purity, ≥ 98.0%; Merck KGaA, CAS-No: 7791-20-0) were used for preparation of artificial solutions by applying distilled water prepared through the standard purification method.

2.2. Methods

2.2.1. Alkaline fusion technique

Synthesis experiments involved an alkaline fusion step, applied before hydrothermal reactions (Kamyab et al., 2020; Ríos et al., 2009).

In doing so, first, 6 g of powdered kaolinite (<~75μm), prepared through grinding by a pestle and mortar then sieving by the usage of <200 mesh sieve, was dry mixed with NaOH powder (raw material/alkaline activator in 1/1.2 weight proportion). Second, the mixture was put in a ceramic crucible and fused at 650°C for 90 minutes in an electric temperature-controlled furnace. Next, the fused mixture was ground by a ceramic mortar and pestle, and the powdered fused mixture was added to distilled water. Further, the suspension was stirred by a magnetic stirrer, for 30 minutes. After 30 minutes, Aluminum Chloride solution was added to the suspension, then stirred for another 30 minutes to obtain a homogeneous gel. Thereafter, the homogeneous gel was poured in stainless steel autoclave and was put in an oven for certain periods of reaction time, 24, 48, 72 and 96 h, at 100, 140, 180 and 220°C.

After reaction time completion, the autoclave was removed from the oven and the product was filtered and washed several times with distilled water to remove the excess alkaline reagent, Finally, the produced material was dried overnight at 80°C and was ground to prepare a powdered sample for further characterizations. A flowchart presenting the synthesis process is demonstrated in Fig. 1.

2.2.2. Batch type experiments

The batch adsorption experiments were conducted (Salih, 2017) to evaluate the capability of synthesized sodalites for Cu^{2+}, Zn^{2+} and Ni^{2+} ions uptake from artificial monometallic solutions. The experiments were performed at room temperature through applying determined dosage of sodalite adsorbents and synthetic solutions containing Cu^{2+}, Zn^{2+} or Ni^{2+} ions (sorbent/solution mixture of 0.5 g/25 mL). In the process, the sorbent/solution samples were poured in 25 mL glass containers; individually, then were kept on a rotary shaker with agitation rate of 30 rpm for time intervals of 1, 2, 4, 8, 12, and 24 h. Then after scheduled periods of time the samples were removed from the shaker and the filtrates were collected through filtration of suspensions. Finally, filtrates pH was measured and final leachates were kept in a refrigerator at 4°C for detection of existing metal ions.

2.2.3. Characterization techniques

The bulk chemical composition of kaolinite raw material was analysed by X-ray fluorescence spectroscopy using an Epsilon 3XLE PANalytical Energy-dispersive spectrometer with a silver anode tube (max. voltage 50 kV, max. 3 mA; max. tube power 15 W) and a high-resolution silicon draft detector (SDD).

The crystalline structures of raw material and synthesized phases were determined by X-ray diffractometry utilizing an Empyrean PANalytical diffractometer with generator setting of 40 mA, 40 kV, Ni-filtered Cu (Kα) radiation and a PIXcel1D detector.

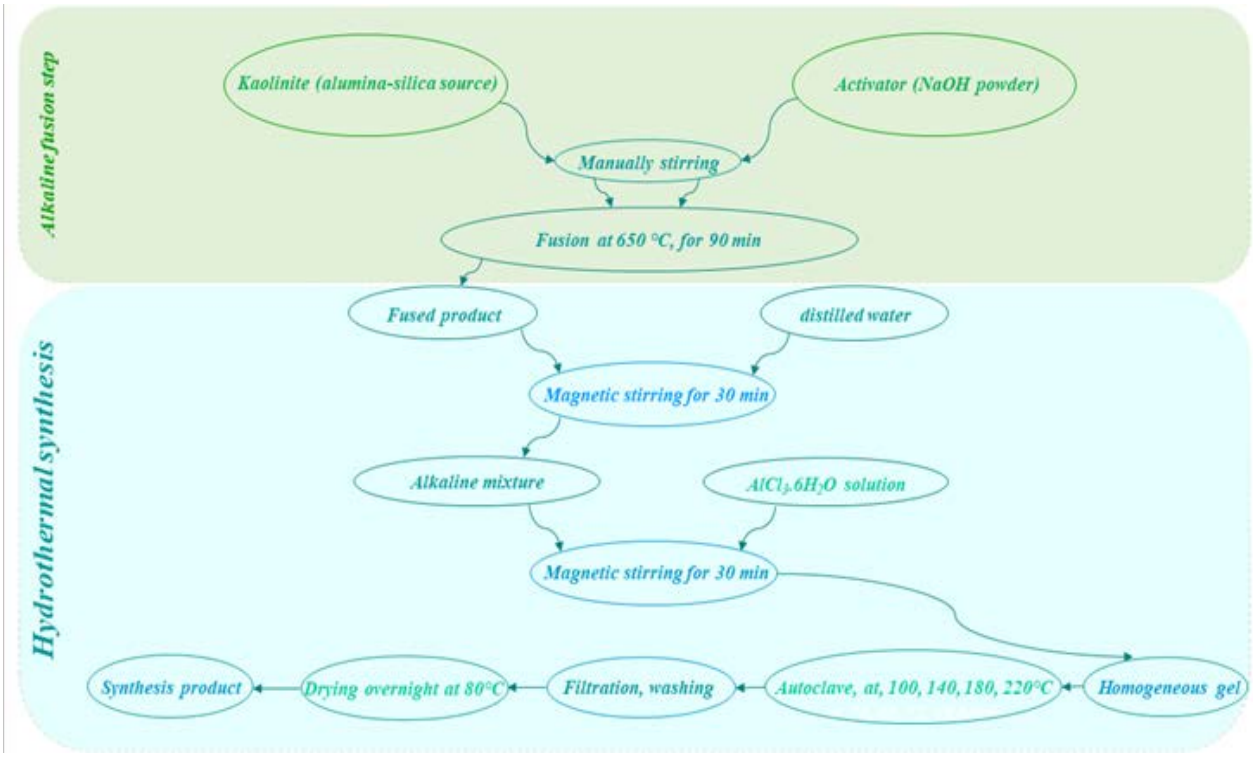

Fig. 1. Processing of kaolinite into synthetic product (Kamyab, 2020)

The morphology and elemental compositions of raw material and products were inspected by SEM and EDS analytical techniques using a ZEISS EVO50 Scanning Electron Microscope equipped with SE1, VPSE detectors. The analyses were performed through applying the analytical conditions of 15, 20 kV ETH, and 7, 8.5 mm AWD. The framework quality of raw material and products was detected by Fourier transform infrared spectroscopy using a Bruker Alpha FT-IR spectroscope equipped with a high sensitivity DLATGS detector. All the measurements were performed via Platinum-ATR single reflection mode and samples were analyzed in the region of 4000-400 cm^{-1}.

The final leachates were taken for determination of the metal ions by Inductively Coupled Plasma-Optical Emission Spectrometry using an Agilent 5100 ICP-OES equipped with a Vista Chip II CCD detector and a solid-state RF generator operating at 27MHz. The measurements were simultaneously carried out over 167 to 785 nm wavelength range.

3. Results and discussion

3.1. Chemical composition of kaolinite

The bulk chemical composition of kaolinite raw material is presented in Table 1. The composition revealed 63wt% silica, and 24wt% alumina verifying the SiO_2/Al_2O_3 ratio equal to 2.62 which is higher than the amount of 1.19, reported by Ríos (2008) for SiO_2/Al_2O_3 ratio.

3.2. Alkaline-fused products

The alkaline fusion products of kaolinite, which are disclosed in Table 2, illustrated as-synthesized zeolitic products consisting of zeolite A, zeolite X, analcime, and cancrinite, formed with sodalite at 100, 180, and 220°C. Besides, sodalite shown to be synthesized as pure phase in 140°C, 220°C.

The results of synthesis experiments displayed formation of zeolite A and zeolite X using 7.32g and 7.72g sodium hydroxide activator at 100°C. Moreover, sodalite was synthesized with quartz and zeolite A, at 100 and 140°C also with cancrinite and analcime at 180 and 220°C. Furthermore, the results substantiated synthesis of sodalites as pure phases at 140°C, using both 7.32g and 7.72g sodium hydroxide activator also at 220°C applying 7.32g NaOH activator.

3.3. Characterization of synthesized sodalites

The X-ray powder diffraction patterns of raw material, SS1, sodalite synthesized at 220°C using 7.32g NaOH, SS2, sodalite synthesized at 140°C applying 7.72g NaOH and SS3, sodalite synthesized at 140°C utilizing 7.32g NaOH, are presented in the Fig. 2. So that, kaolinite and quartz peaks can be detected in XRD pattern of starting material (Fig. 2 (d)), meanwhile no impurity peaks can be seen in the patterns regarding synthesized sodalites (Fig. 2 a, b, c). The SEM images showing the morphology of kaolinite starting material, sodalites synthesized using

7.32g and 7.72g NaOH activator, at 140°C, and sodalite synthesized utilizing 7.32g NaOH activator, at 220°C are displayed in Fig. 3.

The SEM images reveal kaolinite appearing platy shaped particles (Fig. 3(a)), and sodalites presenting spherical shapes: SS1 formed at 220°C applying 7.32g NaOH, (Fig. 3 (b)), SS2 synthesized at 140°C using 7.72g NaOH, (Fig. 3(c)), and SS3 produced at 140°C utilizing 7.32g NaOH, (Fig. 3(d)). In this vein, Shirani Lapari et al. (2015) reported synthesized sodalite showing regular spherical shape which was formed from a mixture of fumed silica and $NaAlO_2$ under hydrothermal conditions using NaOH alkaline solutions.

Table 1. Chemical composition of the Kaolinite determined by XRF

Component	*(wt%)*	*Component*	*(wt%)*
SiO_2	63.36	Ba	0.01
Al_2O_3	24.16	Cl	0.12
Fe_2O_3	0.80	Cr	--
MgO	6.78	Eu	--
CaO	2.32	Mn	0.01
K_2O	0.62	Ni	--
TiO_2	0.02	Sr	0.06
P_2O_5	0.36	LOI[a]	1.38
SO_3	0.00	Total	100

[a]*LOI: Loss-on-Ignition*

Table 2. Alkaline fusion products formed applying various amounts of NaOH activator and $AlCl_3.6H_2O$

NaOH powder (g)	*$AlCl_3.6H_2O$ (N)*	*Temperature (°C)*	*Time (h)*	*Products*
7.32	1	100	24	Zeo A[a], Sdl[b], Zeo X[c]
7.72	2	100	24	Zeo A, Qz[d], Sdl
8.1	3	100	24	Qz, Sdl
7.32	1	140	48	Sdl
7.72	2	140	48	Sdl
8.1	3	140	48	Bay[e], Qz
7.32	1	180	72	Sdl, Anl[f]
7.72	2	180	72	Sdl, Ccn[g]
8.1	3	180	72	Hl[h]
7.32	1	220	96	Sdl
7.72	2	220	96	Sdl, Ccn
8.1	3	220	96	Hl, Zeo A

[a]*Zeo A: Zeolite A,* [b]*Sdl: Sodalite,* [c]*Zeo X: Zeolite X,* [d]*Qz: Quartz,* [e]*Bay: Bayerite,* [f]*Anl: Analcime,* [g]*Ccn: Cancrinite,* [h]*Hl: Halite*

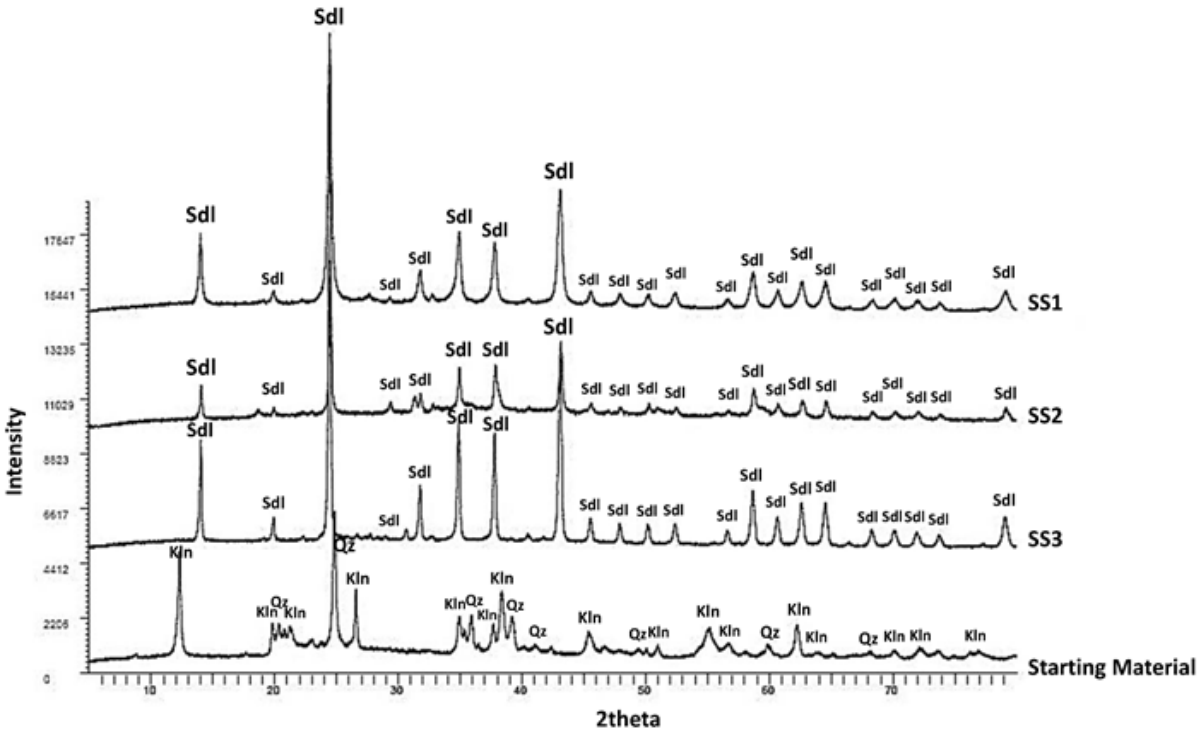

Fig. 2. XRD patterns (**a**) SS1, (**b**) SS2, (**c**) SS3, (**d**) Starting Material; Kln: kaolinite, Qz: quartz, Sdl: sodalite

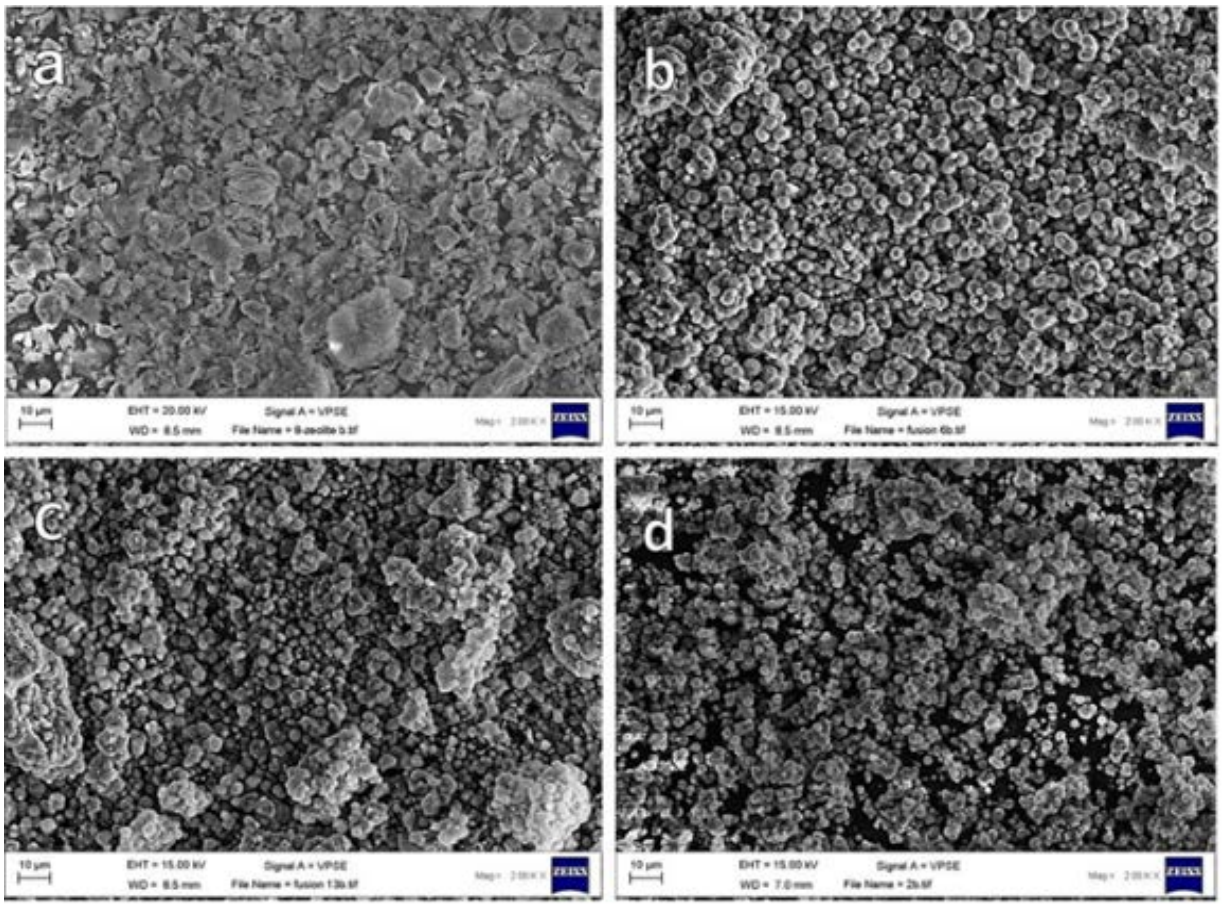

Fig. 3. SEM images (**a**) starting material, (**b**) SS1, (**c**) SS2, (**d**) SS3

The elemental compositions of synthesized sodalites detected by SEM/EDX are shown in Table 3. The elemental compositions obtained via EDX quantitative analysis illustrate almost the same weight percentages of silica and alumina confirming SiO_2/Al_2O_3~1 ratio for the three sodalites. The FTIR patterns of synthesized sodalites and kaolinite raw material are shown in Fig. 4.

Infrared spectrum regarding sodalite synthesized at 220°C, using 7.32g sodium hydroxide activator (Fig. 4(a)), demonstrated O-T-O bending vibrations at 430 and 462 cm^{-1} adsorption bands, also T-O-T, (T=Si, Al) symmetric stretching vibrations at 668, 712, and 735 cm^{-1} adsorption bands, further, asymmetric stretching vibration at 963 cm^{-1} adsorption band. In this context, Yao et al. (2008) reported Si-O-T bending oscillations at 450-475 cm^{-1} adsorption region, the symmetric stretching vibration at around 690 cm^{-1} adsorption band occurred within 660-770 cm^{-1} region, and Si-O-T asymmetric stretching vibrations representing formation of Si-O-Al bonds in sodalite structure observed within 903-948 cm^{-1} adsorption region. The FTIR pattern of sodalite synthesized at 140°C, applying 7.72g NaOH activator (Fig. 4(b)) disclosed O-T-O bending vibrations at the adsorption bands of 429 and 460 cm^{-1}, symmetric stretching oscillations at 669, 712, and 734 cm^{-1} adsorption bands, and the asymmetric stretching vibration at adsorption band of 957 cm^{-1}.

All the same, infrared spectrum of sodalite synthesized at 140°C, utilizing 7.32g sodium hydroxide activator (Fig. 4(c)) revealed O-T-O bending vibrations at 432 and 463 cm^{-1} adsorption bands, T-O-T symmetric stretching vibrations at 668, 712, and 735 cm^{-1} adsorption bands and asymmetric stretching oscillation at adsorption band of 963 cm^{-1}.

Infrared pattern of kaolinite raw material disclosed Si-O stretching vibrations at 426, 457, 1001, 1024, and 1106 cm^{-1} adsorption bands, and Si-O-Al stretching oscillations at adsorption bands of 531, 687, 749, and 795 cm^{-1}. In this spectrum, the inner and outer -OH bending vibrations displayed at 911 and 942 cm^{-1} adsorption bands, respectively.

Meanwhile, -OH groups stretching oscillations in kaolinite structure can be found at adsorption bands of 3619, 3645, and 3689 cm^{-1}. Hereof, Ríos (2008) specified presence of -OH groups stretching vibrations at 3619, 3645, and 3692 cm^{-1}adsorption bands. Even so, Hoch and Bandara (2005) did not observe these bands in infrared spectrum of kaolinite. In subsequence, Van der Marel and Beutelspacher (1976) proved existence of Si-O stretching vibration at 1119 cm^{-1} adsorption band, and Si-O-Si, and Si-O-Al framework oscillations at adsorption bands of 1012 and 1034 cm^{-1}, correspondingly. Besides, Frost et al. (2002) found -OH bending vibrations and surface -OH also inner -OH vibrations at 916 and 942 cm^{-1} adsorption bands, respectively.

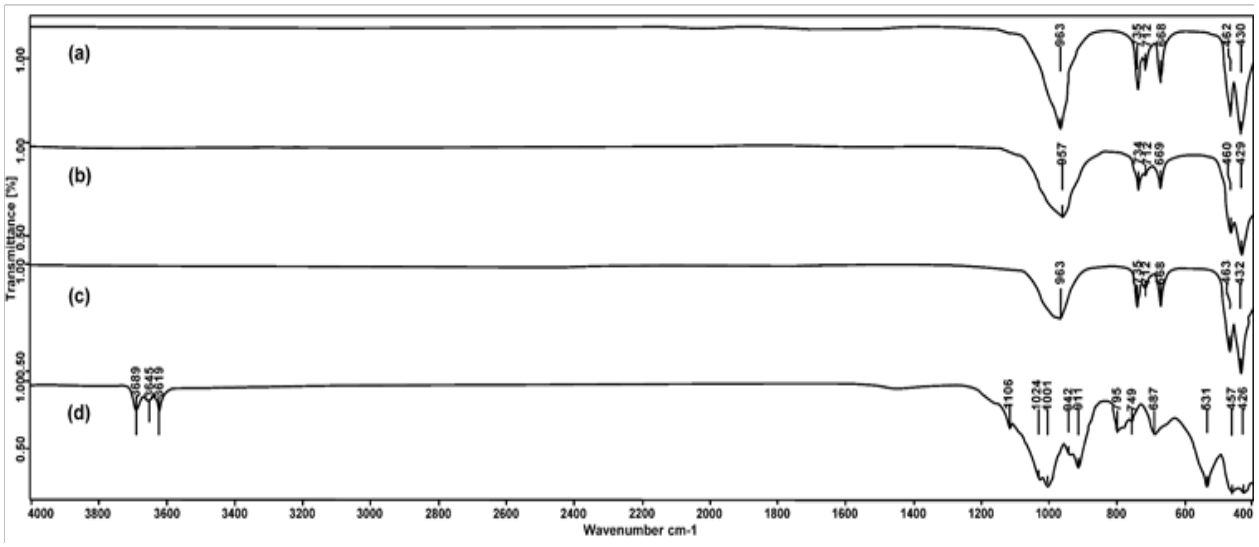

Fig. 4. FTIR patterns (a) SS1, (b) SS2, (c) SS3, (d) kaolinite raw material

Table 3. Elemental compositions of synthesized sodalites: SS1, SS2, and SS3

Elm[a]	***C***	***O***	***Na***	***K***	***Al***	***Si***	***Cl***	***Ca***	***Mg***	***Fe***	***S***
SS1[b]											
											Spt1[c]
Wt%	15.54	48.37	12.32	--	10.07	10.98	2.46	0.26	--	0.04	--
Total	100wt%										
											Spt2
Wt%	15.24	50.69	12.23	0.09	9.12	9.95	2.15	0.25	0.15	0.12	0.01
Total	100wt%										
											Spt3
Wt%	11.99	48.84	13.23	--	11.15	11.93	2.53	0.33	--	--	--
Total	100wt%										
											Spt4
Wt%	16.77	46.91	12.00	0.10	10.18	11.20	2.60	0.24	--	--	--
Total	100wt%										
SS2											
											Spt1
Wt%	28.66	45.50	9.56	--	6.13	7.68	2.00	0.28	--	0.19	--
Total	100wt%										
											Spt2
Wt%	21.78	47.51	10.74	--	7.29	9.56	2.46	0.64	--	0.02	--
Total	100wt%										
											Spt3
Wt%	25.74	45.71	10.51	--	6.81	8.58	2.27	0.37	--	0.01	--
Total	100wt%										
											Spt4
Wt%	18.74	47.29	11.72	--	8.35	10.60	2.81	0.33	--	0.15	0.01
Total	100wt%										
SS3											
											Spt1
Wt%	14.90	50.92	11.82	--	11.02	9.15	2.02	--	--	0.17	--
Total	100wt%										
											Spt2
Wt%	20.79	49.08	10.54	0.04	9.44	7.95	1.65	0.09	0.12	0.16	0.14
Total	100wt%										
											Spt3
Wt%	17.39	51.07	10.85	0.15	10.33	8.34	1.31	0.06	0.18	0.19	0.13
Total	100wt%										
											Spt4
Wt%	11.16	52.07	13.11	--	11.17	10.15	2.19	0.07	--	0.08	--
Total	100wt%										

[a]Elm: Element; *[b]SS1: Synthesized Sodalite 1;* *[c]Spt1: Spectrum 1*

3.4. Synthesis conditions investigation

The synthesis experiments in the present study verified zeolite A formation along with zeolite X, at 100°C. This result can be corroborated by the outcomes substantiating zeolite A synthesis with ideal ratio of Si/Al=1, at 100°C (Mgbemere et al., 2018; Ríos et al., 2010). All the same, the current study results verified synthesis of zeolite A together with Halite, at 220°C. In this connection, Salih (2017) reported synthesis of cubic-shaped zeolite A with more than 90% crystallinity, at 200°C. In this work, sodalite was synthesized with cancrinite, and analcime, at 180°C and 220°C also at 180°C. Similarly, Passos et al. (2017) confirmed formation of sodalite together with cancrinite and analcime in temperature range of 150-230°C. In current research, sodalite was formed as pure phases at 140°C, and 220°C. On this matter, Li et al. (2015) synthesized sodalite as pure phase, at 160°C.

Theoretically, high alkalinity condition causes high concentration of OH^- ion which leads to a less possibility for zeolite crystallization. Otherwise, high level of alkalinity results in low stability of Si-Al bonds in an aluminosilicate framework; therefore, there would be a small synthesized product.

Accordingly, in high alkaline conditions; subsequently, high OH^- ion concentrations, crystallization of sodalite as pure phase is almost inaccessible. This substantiates the essential influence of reaction medium alkalinity on the synthesis of sodalite (Sari et al., 2018).

3.5. Adsorption experiments evaluation

The adsorption experiments were performed at room temperature, during the course of 1-24 h. The ICP-OES analysis was used to quantify the concentrations of Cu^{2+}, Zn^{2+} and Ni^{2+} ions in resulting filtrates. The percentage removal efficiency (R%) was calculated via the following equation (Eq. 1).

$$R\% = (C_O - C_e)/C_O \times 100 \quad (1)$$

where: C_0 and C_e are the initial and equilibrium concentrations of adsorbate (mg L^{-1}), respectively.

The amount of adsorbate adsorbed at different time intervals was calculated by Eq. (2) (Nethaji et al., 2013).

$$Q_t = ((C_O - C_t)/W) \times V \quad (2)$$

where: Q_t is the amount of adsorbate adsorbed at any time t, C_0 and C_t (mg L^{-1}), are adsorbate concentrations at initial time and time t (min), respectively. V is the volume of adsorbate solution (L), and W is the amount of adsorbent used (g).

The patterns presenting the uptake percentages of Cu^{2+}, Zn^{2+} and Ni^{2+} ions versus given contact time and plots revealing the amounts of Cu^{2+}, Zn^{2+} and Ni^{2+} ions adsorbed at different time intervals versus time are shown in the Figs. (5-7).

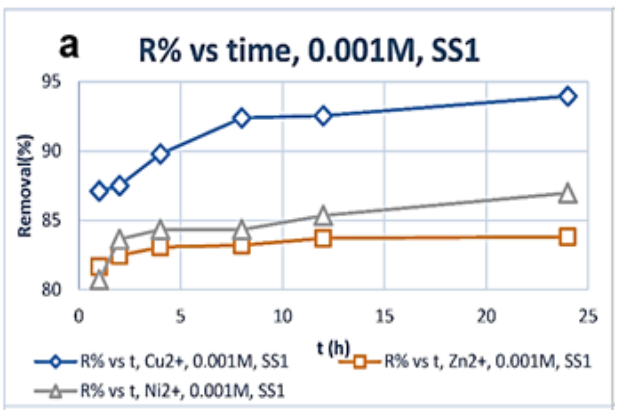

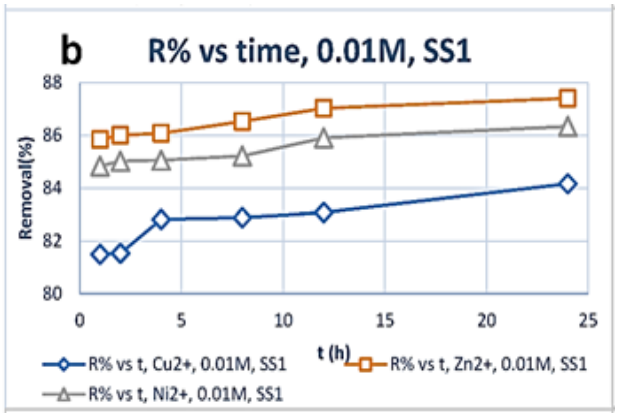

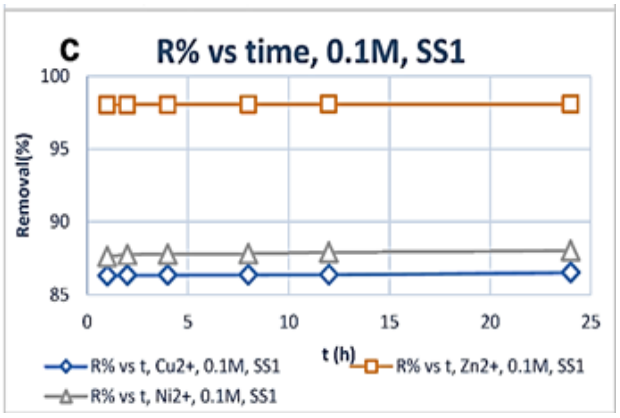

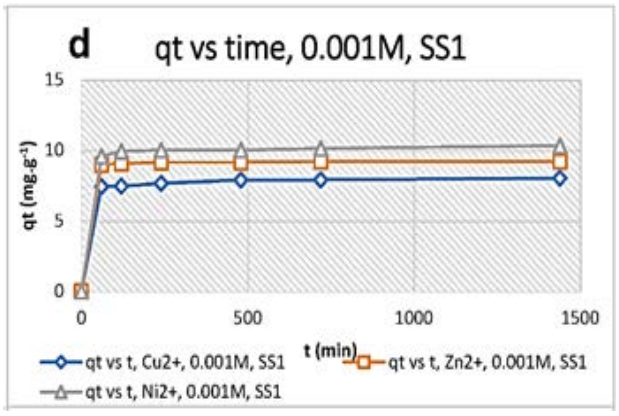

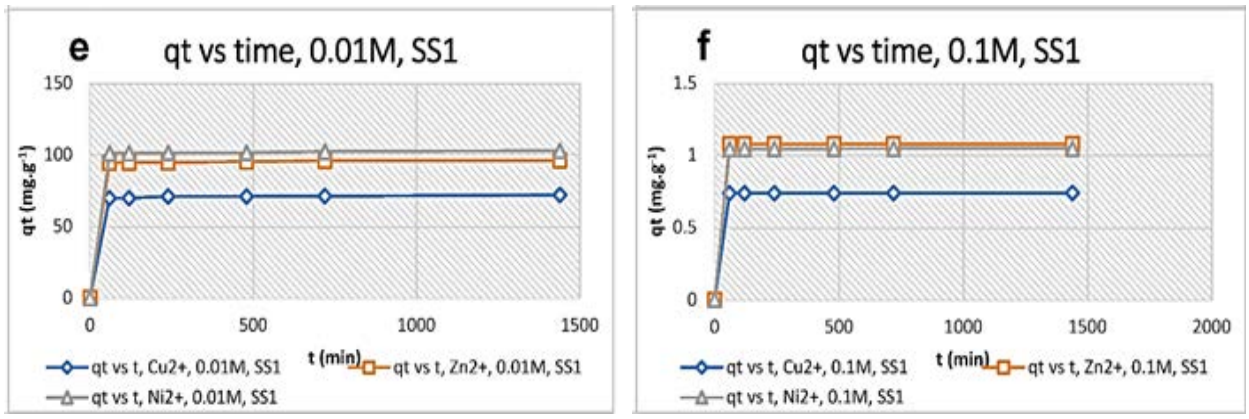

Fig. 5. (a), (b), (c) R % vs time and (d), (e), (f) Qt vs time for 0.001M, 0.01M, 0.1M solutions, SS1

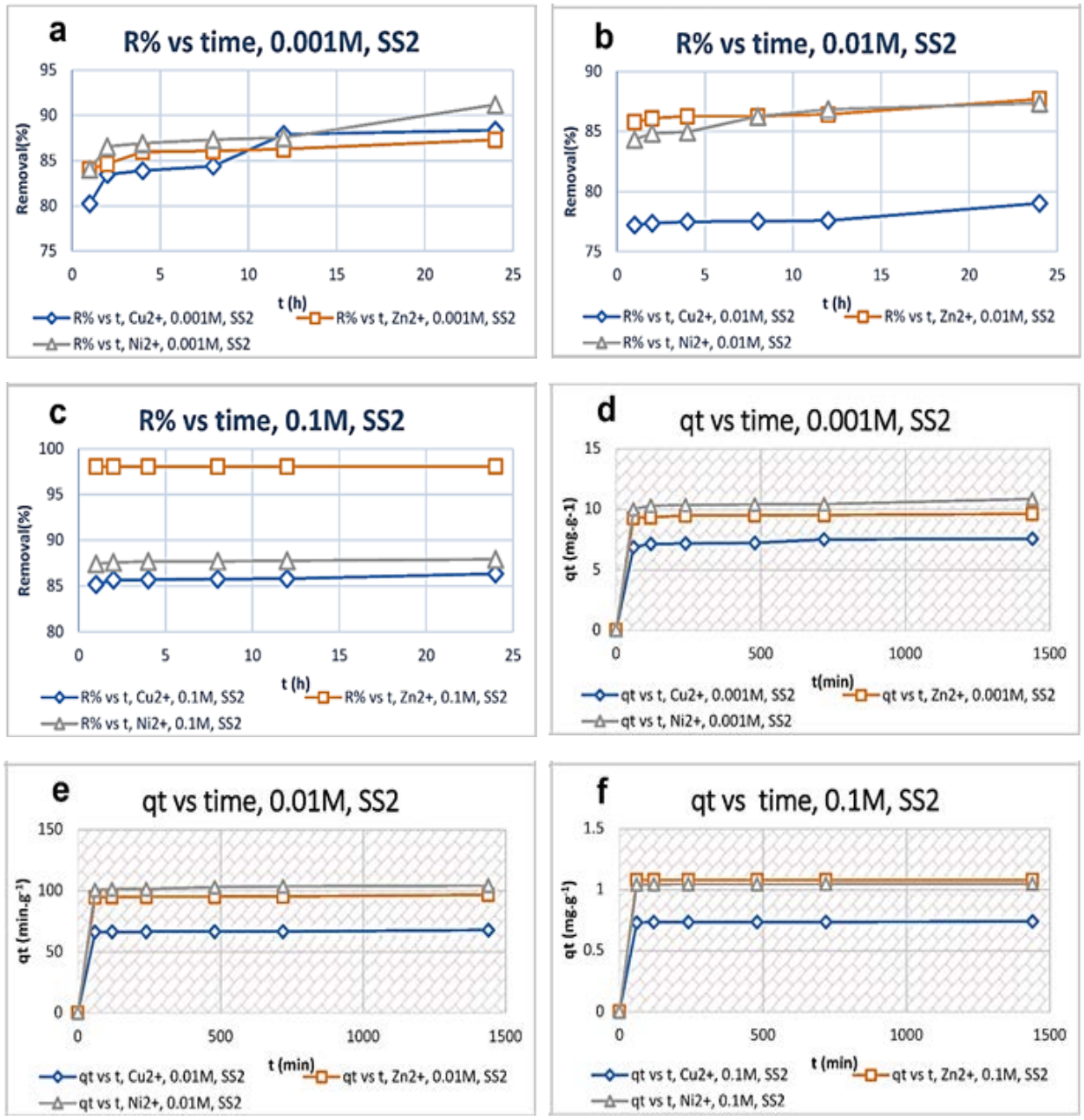

Fig. 6. (a), (b), (c) R % vs time and (d), (e), (f) Qt vs time for 0.001M, 0.01M, 0.1M solutions, SS2

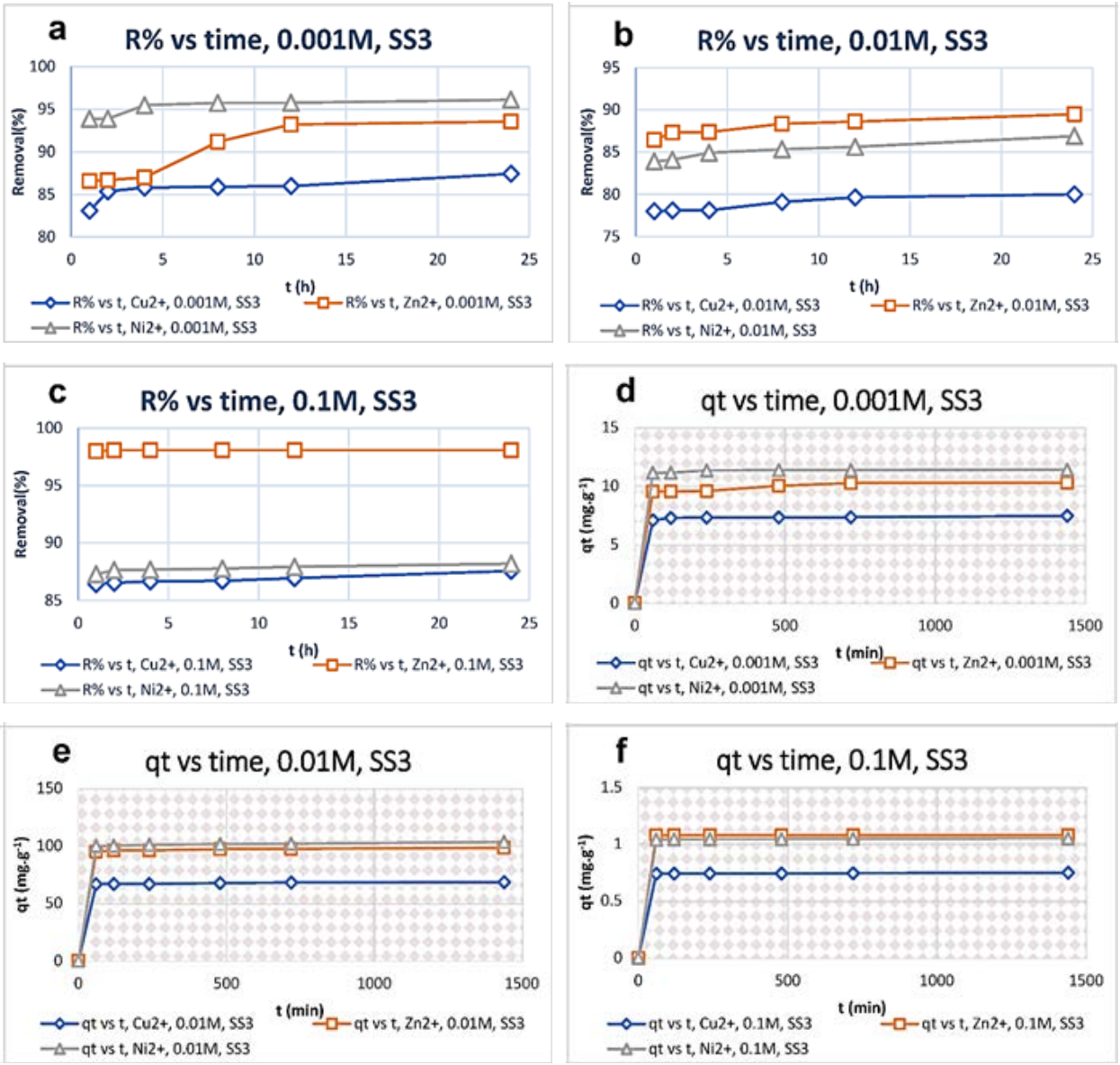

Fig. 7. (a), (b), (c) R % vs time and (d), (e), (f) Qt vs time for 0.001M, 0.01M, 0.1M solutions, SS3

The results of ICP-OES analysis (Figs. 5 (a, b, c), 6 (a, b, c), and 7 (a, b, c)), obtained using 0.001M solutions, indicated that SS1 demonstrated higher affinity for Cu^{2+} ion than Ni^{2+} and Zn^{2+} ions, SS2 preferentially adsorbed Ni^{2+} ion higher than Zn^{2+} and Cu^{2+} ions, and SS3 removed Ni^{2+} ion much more than Zn^{2+} and Cu^{2+} ions. Considering the adsorption percentage, SS1 cleaned up Cu^{2+} ion between 87.12% and 93.96%, Zn^{2+} ion from 81.65% to 83.80%, and Ni^{2+} ion within the range of 80.70%-86.97%. SS2 adsorbed 80.22%-88.34% amount of Cu^{2+} ion, from 84.05% to 87.28% percentage of Zn^{2+} ion, and 84.03%-91.17% percent of Ni^{2+} ion. SS3 removed 83.07%-87.42% of Cu^{2+} ion, 86.55%-93.52% of Zn^{2+} ion, and 93.84%-96.09% of Ni^{2+} ions, in the period of 1-24 h.

Getting exposure to 0.01M solutions, SS1, SS2, and SS3 preferably adsorbed Zn^{2+} and Ni^{2+} ions higher than Cu^{2+} ion. Regarding the adsorption percentage, SS1 removed Cu^{2+} ion from 81.50% to 84.16%, Zn^{2+} ion within the ranges of 85.83%-87.40%, and Ni^{2+} ion between 84.83% and 86.33%. SS2 adsorbed 77.21%-79.02% of Cu^{2+} ion, 85.78%-87.69% of Zn^{2+} ion, and 84.32%-87.35% of Ni^{2+} ion. SS3 cleaned up Cu^{2+} ion within the range of 78.001%-79.99%, Zn^{2+} ion between 86.41% and 89.47%, and Ni^{2+} ion within the percentages of 83.87%-86.88%, during 1-24 h.

By the usage of 0.1M solutions, SS1, SS2, and SS3 displayed greater adsorption efficiency for Zn^{2+} ion than Cu^{2+} and Ni^{2+} ions. In terms of adsorption percentage, the results disclosed that SS1 clean up 86.31%-86.54% of Cu^{2+} ion, 98.03%-98.07% of Zn^{2+} ion, and 87.63%-88.03% of Ni^{2+} ion. SS2 removed Cu^{2+} ion within the range of 85.15%-86.31%, Zn^{2+} ion within the percentages of 98.04%-98.05%, and Ni^{2+} ion between 87.39% and 87.88%. SS3 adsorbed Cu^{2+} ion from 86.42% to 87.56%, Zn^{2+} ion within the percentages of 97.98%-98.07%, and Ni^{2+} ion between 87.28% and 88.19%, in the course of 1-24 h.

The patterns depicted Q_t versus time (Figs. 5 (d, e, f), 6 (d, e, f), and 7 (d, e, f), demonstrated that

exposing to 0.001M, 0.01M, and 0.1M solutions, the adsorption was rapid in the first 60 minutes, and within 77.212%-98.074% of total adsorption capacity was attained during this period of time. Further, the equilibrium can be obtained almost within 120-240 minutes.

3.6. Adsorption progress and mechanism

The adsorption results verified removal of a significant amount of Cu^{2+}, Zn^{2+} and Ni^{2+} ions at the beginning of the uptake process. So that, during the first 1h, for above 98% of the metal ions was expeditiously cleaned up from artificially polluted solutions through being adsorbed on the active sites available on the sodalite surface. However, with an increase in processing time, the number of active sites for the adsorption gradually decreased and the removal rate slightly declined, then the process continued until equilibrium conditions were reached in the period of 2-4 h. On this matter, Irannajad et al. (2016) reported a rapid adsorption of Cu^{2+}, Zn^{2+}, and Cd^{2+} ions for more than 90% within 60 min, which over time became less and slower, then reached a steady state.

The results demonstrated that heavy metal ions removal mainly depends on the initial metal ions concentration in the solution. Metal ions sorption initially increases with an increase in metal ions concentration in solution, then becomes saturated after a certain concentration of metal ions (Mehta and Gaur, 2001a, 2001b, 2001c; Mehta et al., 2002a, 2002b). Since the adsorbent surface where the adsorption occurred reaches to its maximum uptake, so that no more metal ions can be adsorbed (Taamneh and Sharadqah, 2017). At lower concentrations, the ratio of initial metal ions to the available surface area is low; consequently, fractional sorption becomes independent of the initial concentration. However, at higher concentrations, the sites available for sorption become fewer compared to the metal ions present; accordingly, the binding of the metal ions is greatly dependent upon the initial concentration. Horsfall et al. (2006) specified when the initial concentration increases, the removal rate decreases. Because, at higher concentration, the number of metal ions competing for the available binding sites on the adsorbent surface increases and therefore reduces the number of binding sites. Indeed, at higher concentration, the average distance between the adsorbed metal ions will be reduced. Thus, the ability of metal ions to migrate to the adsorbent surface decreases. Subsequently, the high initial concentration accelerates a driving force and attenuates the mass transfer resistance (Wang et al., 2015). The driving force in an ion-exchange process; presumably, arises from the fact that metal ions in more concentrated solutions are more readily adsorbed by zeolite (Ostroski et al., 2007).

Offering mobility of the alkali and alkaline earth metal ions (Rad et al., 2014; Yurekli, 2016) enables zeolites to compensate net negative charge resulting from Si^{4+} and Al^{3+} cations substitution in their framework. This introduces Na^{+}, K^{+} or Ca^{2+} ions, in most cases, and Li^{+}, Mg^{2+}, Sr^{2+} or Ba^{2+} ions, in some cases (Armbruster and Gunter, 2001), into zeolites cavities as exchangeable counterions being weakly bound with aluminosilicate structure (Farkaš et al., 2005; Widiastuti et al., 2011). Additionally, H_2O molecules (OH^{-} ions) being retained in the cavities are able to involved in ion exchange reactions (Salih, 2017). Taking this into consideration, Cu^{2+}, Zn^{2+} and Ni^{2+} ions can substitute into the structures of zeolites, as they come in contact with the aqueous contaminant solutions.

In fact, the uptake of heavy metal ions is succinctly attributed to both mechanisms of ion exchange and the adsorption process (Ćurković et al., 1997). The phenomenon of loading metal ions can be described as three stages. So that, the first stage involves a fast metal ions intake appertaining to the ion exchange in the micropores on the microcrystal surfaces of the adsorbent. The second stage involves an inversion of ion exchange occurred due to the counter diffusion of exchangeable cations. The third stage is described as adsorption of metal ions but at a much slower rate compared to the first stage (Sprynskyy et al., 2006).

3.7. Adsorption isotherms and kinetics

Adsorption isotherms represent the amount of adsorbate adsorbed per unit weight of adsorbent (Mall et al., 2006). The adsorption isotherms can be assessed for sake of their correlation for experimental data regarding the effluents removal from the system. In view of this, the adsorption isotherm models chosen to be scrutinized for their agreements with the adsorption data in current study were Langmuir and Freundlich isotherms which are expressed as following equations, (Eq. 3) (Dada et al., 2012) and (Eq. 4) (Kumar et al., 2010), individually.

$$1/Q_e = 1/Q_m + 1/Q_m K_L C_e \quad (3)$$

where: Q_e is the amount of adsorbate adsorbed on the adsorbent surface at equilibrium (mg g^{-1}), K_L is Langmuir constant which is related to the energy of adsorption (L mg^{-1}), C_e is unabsorbed adsorbate concentration at equilibrium (mg L^{-1}), and Q_m is maximum monolayer coverage capacity (mg g^{-1}).

$$\log Q_e = \log K_F + 1/n \cdot \log \cdot C_e \quad (4)$$

where: K_F is the Freundlich constant indicative of the adsorption capacity of the adsorbent (mg g^{-1} (L mg^{-1})$^{(1/n)}$), and *1/n* is a function of adsorption intensity. The values of correlation coefficient and constants of Langmuir and Freundlich models are summarized in Table 4.

The obtained correlation coefficients (R^2) indicated the suitability of fit considering the point that, larger values are better (Tohdee et al., 2018). It was found that, the experimental data for Cu^{2+}, Zn^{2+}

and Ni^{2+} ions adsorption were satisfactorily represented by the Freundlich model, indicating heterogeneous nature of adsorption surface on the sodalites. So that, the Freundlich model provided the best fit of adsorption isotherms for aforesaid metal ions with correlation coefficients varying as 0.9848-0.9995, 0.9980-0.9999, and 0.9996-1.0000, for using 0.001M, 0.01M, and 0.1M solutions, respectively. 1/n is a heterogeneity parameter (Doke et al., 2013) indicating that the smaller 1/n, the greater the expected heterogeneity. If value of *1/n* is below one, it indicates a normal adsorption (Dada et al., 2012). The values of 1/n ranging as 0.0535-0.2083, 0.1362-0.2793, and 0.0198-0.1664, for applying 0.001M, 0.01M, and 0.1M solutions, individually, verified a favorable adsorption in this study.

Adsorption kinetics studies provide information required to understand the dynamic interactions of pollutants with adsorbents and to predict their rate with time. In this work, pseudo-first-order and pseudo-second-order kinetic models were applied to the adsorption data to evaluate the controlling mechanism of adsorption processes such as mass transfer and chemical reaction, and to identify the potential rate controlling steps. The pseudo-first-order and pseudo-second-order kinetic models are described as following equations, Eq. (5) and Eq. (6), correspondingly (Javadian et al., 2015).

$$\ln(Q_e - Q_t) = \ln Q_e - k_1 t \quad (5)$$

where Q_e and Q_t (mg g^{-1}) represent the amount of adsorbate adsorbed at equilibrium and at given time *t*, respectively. *t* is time (min), and k_1 is the rate constant (min^{-1}) of pseudo-first-order kinetic model.

$$t/Q_t = 1/(k_2 Q_e^{\,2}) + (1/Q_e)t \quad (6)$$

where k_2 is the rate constant (g mg^{-1} min^{-1}) of pseudo-second-order kinetic model.

The calculated parameters of the pseudo-first-order and pseudo-second-order kinetic models are presented in Table 5.

Table 4. Langmuir and Freundlich isotherms parameters

SS[a]	***Metal ion***	***Langmuir Isotherm***			***Freundlich Isotherm***		
		Q_m (mg g^{-1})	***K_L (L mg^{-1})***	***R^2***	***K_F (mg g^{-1} (L mg^{-1}) $^{(1/n)}$)***	***1/n***	***R^2***
0.001M solutions							
SS1	***Cu^{2+}***	13.4149	0.1440	0.9628	6.3154	0.1019	0.9895
	Zn^{2+}	11.0734	0.1380	0.9986	4.3715	0.2083	0.9995
	Ni^{2+}	13.0224	0.1230	0.9786	5.3500	0.1912	0.9925
SS2	***Cu^{2+}***	9.7999	0.1670	0.9746	4.4325	0.1773	0.9901
	Zn^{2+}	12.2805	0.1270	0.9947	5.4792	0.1678	0.9983
	Ni^{2+}	15.4989	0.1100	0.9581	7.1873	0.1340	0.9848
SS3	***Cu^{2+}***	9.5458	0.1660	0.9872	4.3808	0.1733	0.9958
	Zn^{2+}	16.6569	0.1130	0.9803	7.7162	0.1075	0.9944
	Ni^{2+}	24.6249	0.0930	0.9914	10.1103	0.0535	0.9979
0.01M solutions							
SS1	***Cu^{2+}***	86.5872	0.0179	0.9972	22.2940	0.2088	0.9990
	Zn^{2+}	123.8996	0.0124	0.9992	40.2286	0.1546	0.9997
	Ni^{2+}	129.3662	0.0118	0.9994	38.7525	0.1684	0.9998
SS2	***Cu^{2+}***	76.4112	0.0208	0.9998	13.0354	0.2793	0.9999
	Zn^{2+}	125.2202	0.0123	0.9986	41.2078	0.1515	0.9995
	Ni^{2+}	133.3120	0.0117	0.9975	40.5469	0.1647	0.9992
SS3	***Cu^{2+}***	78.0869	0.0202	0.9996	14.3382	0.2674	0.9998
	Zn^{2+}	133.9278	0.0119	0.9937	46.7846	0.1362	0.9980
	Ni^{2+}	131.3278	0.0118	0.9953	38.6274	0.1712	0.9984
0.1M solutions							
SS1	***Cu^{2+}***	0.9375	1.6100	1	0.6476	0.1570	1
	Zn^{2+}	3.7656	0.9470	1	1.0949	0.0198	1
	Ni^{2+}	1.3774	1.1100	0.9999	0.9051	0.1385	1
SS2	***Cu^{2+}***	0.9292	1.6300	0.9989	0.6390	0.1664	0.9996
	Zn^{2+}	3.7438	0.9470	1	1.0946	0.0199	1
	Ni^{2+}	1.3712	1.1100	0.9998	0.8997	0.1410	0.9999
SS3	***Cu^{2+}***	0.9693	1.5800	0.9994	0.6673	0.1493	0.9998
	Zn^{2+}	3.7592	0.9480	1	1.0951	0.0201	1
	Ni^{2+}	1.3844	1.1100	0.9993	0.9073	0.1397	0.9998

[a]*SS: Synthetized Sodalite*

Table 5. Pseudo-First-Order and Pseudo-Second-Order kinetics parameters

SS[a]	Metal ion	Pseudo-first-order model			Pseudo-second-order model		
		k_1 (min^{-1})	Qe ($mg\ g^{-1}$)	R^2	k_2 ($g\ mg^{-1}\ min^{-1}$)	Qe ($mg\ g^{-1}$)	R^2
0.001M solutions							
SS1	Cu^{2+}	0.0008	1.1987	0.7663	1.2261	8.8699	1
	Zn^{2+}	0.0007	1.0042	0.6468	0.2642	13.0421	1
	Ni^{2+}	0.0008	1.0859	0.7134	0.8718	11.5284	0.9999
SS2	Cu^{2+}	0.0008	1.2859	0.7434	1.5999	8.1951	0.9998
	Zn^{2+}	0.0007	1.0328	0.7688	0.5136	11.5902	1
	Ni^{2+}	0.0008	1.1212	0.8566	1.2360	11.6947	0.9995
SS3	Cu^{2+}	0.0008	1.2503	0.6385	0.7766	8.7784	0.9999
	Zn^{2+}	0.0008	1.0585	0.7729	1.1621	11.1987	0.9999
	Ni^{2+}	0.0009	1.2422	0.5920	0.2112	16.2131	1
0.01M solutions							
SS1	Cu^{2+}	0.0060	7.7428	0.8338	0.0706	89.6674	1
	Zn^{2+}	0.0080	10.4737	0.9236	0.0324	133.6341	1
	Ni^{2+}	0.0085	11.1995	0.9335	0.0328	140.9508	1
SS2	Cu^{2+}	0.0057	7.2996	0.8998	0.0800	83.1623	0.9999
	Zn^{2+}	0.0080	10.4616	0.9263	0.0476	124.1486	0.9999
	Ni^{2+}	0.0085	11.1764	0.8459	0.0497	131.9836	1
SS3	Cu^{2+}	0.0057	7.3892	0.8587	0.0626	87.5524	1
	Zn^{2+}	0.0081	10.5974	0.8660	0.0504	125.2292	1
	Ni^{2+}	0.0084	11.0969	0.9400	0.0586	128.2887	0.9999
0.1M solutions							
SS1	Cu^{2+}	0.0077	12.2321	0.9343	0.7455	2.0795	1
	Zn^{2+}	0.0052	8.3637	0.8099	0.0587	18.1129	1
	Ni^{2+}	0.0053	8.6357	0.8780	0.6280	2.6392	1
SS2	Cu^{2+}	0.0078	12.3652	0.7993	2.7493	1.0998	1
	Zn^{2+}	0.0052	8.3637	0.9418	0.0318	32.5235	1
	Ni^{2+}	0.0054	8.6557	0.8182	0.7140	2.4457	1
SS3	Cu^{2+}	0.0077	12.2208	0.9841	3.6165	1.0233	1
	Zn^{2+}	0.0052	8.3637	0.2585	0.0252	40.7597	1
	Ni^{2+}	0.0054	8.6576	0.8359	1.3590	1.7846	1

[a]*SS: Synthetized Sodalite*

The results indicated that pseudo-second order equation correlated well with adsorption data considering the obtained correlation coefficients (R^2) ranging as 0.9995-1.0000, 0.9999-1.0000, and 1.0000-1.0000 for using 0.001M, 0.01M, 0.1M solutions, respectively. Such adsorption behavior may involve electron-sharing among transition metal ions and the adsorbent (King et al., 2006). Thus, pseudo-second order kinetic model, relying on the assumption that chemisorption may be the rate-limiting step, well described the data for Cu^{2+}, Zn^{2+} and Ni^{2+} ions adsorption.

4. Conclusions

Synthesis of pure phases of sodalites through the alkaline fusion technique confirmed high effectiveness of applying alkaline fusion step before the hydrothermal reactions. This can be due to the certain effect of alkaline fusion process through which the inert crystalline phases present in raw material can fully react, and subsequently results in formation of the highly pure products.

The efficiency of synthesized sodalites for Cu^{2+}, Zn^{2+}, and Ni^{2+} ions removal from aqueous solutions was evaluated via setting batch adsorption experiments. The results demonstrated a rapid adsorption of the metal ions in huge amounts during the first 1 h, which decreases upon approaching equilibrium within 2-4 h.

In addition, the parameters of adsorption isotherms denoted fitness of adsorption data to the Freundlich model which affords the best correlation coefficients indicating adsorption heterogeneous surface phenomenon. Finally, the kinetics data regarding Cu^{2+}, Zn^{2+} and Ni^{2+} ions removal followed the pseudo-second-order model, which suggests chemisorption as the rate limiting step in the adsorption process.

To wrap it up, owing to their potential to act as adsorbents and ion exchangers, the synthesized sodalites can be fruitfully used in environmental applications. Moreover, besides their potential to act as catalysts, their capability of being regenerated after the ion exchange reactions causes them to be influentially employed in industrial applications such

as purification of water sources. Additionally, it is strongly recommended to carry out researches on synthesis of ion-exchanged sodalites and investigation into their remediation efficiencies in further adsorption studies.

Acknowledgements

The authors would like to thank colleagues with different technical expertise who assisted Mr. David Townrow (XRF & XRD), Mrs. Diane Spencer (ICP-OES & FTIR), and Dr. Keith R. Jones (SEM/EDX). Further we would like to acknowledge the administrative assistance offered by the School of Applied Science of the University of Wolverhampton.

References

Anyanwu B.O., Ezejiofor A.N., Igweze Z.N., Orisakwe O.E., (2018), Heavy metal mixture exposure and effects in developing nations: An update, *Toxics*, **6**, 65-97.

Armbruster T., Gunter M.E., (2001), Crystal structures of natural Zeolites, *Reviews in Mineralogy and Geochemistry*, **45**, 1-67.

Babel S., Kurniawan T.A., (2003), Low-cost adsorbents for heavy metals uptake from contaminated water: A review, *Journal of Hazardous Materials*, **97**, 219-243.

Barakat M.A., (2011), New trends in removing heavy metals from industrial wastewater, *Arabian Journal of Chemistry*, **4**, 361-377.

Blázquez G., Calero M., Trujillo C., Martín-Lara M.A, Ronda A., (2018), Binary biosorption of Cu(II)-Pb(II) mixtures onto pine nuts shell in batch and packed bed systems, *Environmental Engineering and Management Journal*, **17**, 1349-1361.

Colella C., (2005), *Natural Zeolites*, In: *Zeolites and Ordered Mesoporous Materials: Progress and Prospects*, Čejka J., Van Bekkum H. (Eds.), 1st FEZA School of zeolite, Prague, Elsevier, Amsterdam, 13-40.

Ćurković L., Cerjan-Stefanović Š., Filipan T., (1997), Metal ion exchange by natural and modified zeolites, *Water Research*, **31**, 1379-1382.

Dada A.O., Olalekan A.P., Olatunya A.M., Dada O., (2012), Langmuir, Freundlich, Temkin and Dubinin-Radushkevich isotherms studies of equilibrium sorption of Zn^{2+} onto phosphoric acid modified rice husk, *IOSR Journal of Applied Chemistry (IOSR-JAC)*, **3**, 38-45.

Denkhause E., Salnikov K., (2002), Nickel essentiality, toxicity and carcinogenicity, *Critical Reviews in Oncology/Hematology*, **42**, 35-56.

Doke K.M., Chavan M., Nalawade R., Khan E.M., (2013), Kinetics and equilibrium isotherm for adsorption of Basic Blue 9 Dye onto activated charcoal prepared from bhagar seed husk, *Journal of Materials and Environmental Science*, **4**, 374-383.

Farkaš A., Rožić M., Barbarić-Mikočević Ž., (2005), Ammonium exchange in leakage waters of waste dumps using natural zeolite from the Krapina region, Croatia, *Journal of Hazardous Materials*, **117**, 1, 25-33.

Frost R.L., Mako E., Kristof J., Kloprogge J.T., (2002), Modification of kaolinite surfaces through mechanochemical treatment-a mid-IR and near-IR spectroscopic study, *Spectrochimica Acta Part A: Molecular and Biomolecular Spectroscopy*, **58**, 13, 2849-2859.

Godiya B.C., Cheng X., Deng G., Li D., Lu X., (2019a), Silk fibroin/polyethyleneimine functional hydrogel for metal ion adsorption and upcycling utilization, *Journal of Environmental Chemical Engineering*, **7**, 102806, https://doi.org/10.1016/j.jece.2018.11.050

Godiya B.C., Cheng X., Li D., Chen Z., Lu X., (2019b), Carboxymethyl cellulose/polyacrylamide composite hydrogel for cascade treatment/reuse of heavy metal ions in wastewater, *Journal of Hazardous Materials*, **364**, 28-38.

Godiya B.C., Liang M., Mir Sayed S., Li D., Lu X., (2019c), Novel alginate/polyethyleneimine hydrogel adsorbent for cascaded removal and utilization of Cu^{2+} and Pb^{2+} ions, *Journal of Environmental Management*, **232**, 829-841.

Godiya B.C., Mir Sayed S., Xiao Y., Lu X., (2020), Highly porous egg white/polyethyleneimine hydrogel for rapid removal of heavy metal ions and catalysis in wastewater, *Reactive and Functional Polymers*, **149**, 104509, https://doi.org/10.1016/j.reactfunctpolym.2020.104509

Hoch M., Bandara A., (2005), Determination of the adsorption process of tributyltin (TBT) and monobutyltin (MBT) onto kaolinite surface using Fourier transform infrared (FTIR) spectroscopy, *Colloids and Surfaces A: Physicochemical and Engineering Aspects*, **253**, 117-124.

Horsfall M., Ogban F., Akporhonor E.E., (2006), sorption of chromium (VI) from aqueous solution by cassava (Manihot sculenta Cranz) waste biomass, *Chemistry & Biodiversity*, **3**, 161-174.

Huang D.L., Zeng G.M., Xu P., Zhao M.H., Lai C., Li N.J., Huang C., Zhang C., Cheng M., (2018), Biosorption behavior of immobilized *Phanerochaete chrysosporium* for heavy metals removal, *Environmental Engineering and Management Journal*, **17**, 12, 2789-2794.

Irannajad M., Kamran Haghighi H., Soleimanipour M., (2016), Adsorption of Zn^{2+}, Cd^{2+}, and Cu^{2+} on zeolites coated by manganese and iron oxides, *Physicochemical Problems of Mineral Processing*, **52**, 894-908.

Javadian H., Ghorbani F., Tayebi H-A., Asl S.M.H., (2015), Study of the adsorption of Cd (II) from aqueous solution using zeolite-based geopolymer, synthesized from coal fly ash; kinetic, isotherm and thermodynamic studies, *Arabian Journal of Chemistry*, **8**, 837-849.

Kamyab S.M., (2020), *Comparative study on hydrothermal transformations of sepiolite and kaolinite (nano layered minerals) and their application in environmental processes*, PhD Thesis, University of Tehran, Iran.

Kamyab S.M., Modabberi S., Williams C.D., Badiei A., (2020), Synthesis of sodalite from sepiolite by alkali fusion method and its application to remove Fe^{3+}, Cr^{3+}, and Cd^{2+} from aqueous solutions, *Environmental Engineering Science*, **37**, 10, DOI: 10.1089/ees.2019.0492.

Khan M.N., Wahab M.F., (2007), Characterization of chemically modified corncobs and its application in the removal of metal ions from aqueous solution, *Journal of Hazardous Materials*, **141**, 237-244.

King P., Srinivas P., Prasanna Kumar Y., Prasad V.S.R.K., (2006), Sorption of copper (II) ion from aqueous solution by Tectona grandis 1.f. (teak leaves powder), *Journal of Hazardous Materials*, **136**, 560-566.

Kumar P.S., Vincent C., Kirthika K., Kumar K.S., (2010), Kinetics and equilibrium studies of Pb^{2+} ion removal from aqueous solutions by use of nano–silversol–coated activated carbon, *Brazilian Journal of Chemical Engineering*, **27**, 339-346.

Li J., Zeng X., Yang X., Wang C., Luo X., (2015), Synthesis of pure sodalite with wool ball morphology from alkali fusion kaolin, *Materials Letters*, **161**, 157-159.

Llanos R.M., Mercer J.F., (2002), The molecular basis of copper homeostasis copper-related disorders, *DNA and Cell Biology*, **21**, 259-270.

Mall I.D., Srivastava V.C., Agarwal N.K., (2006), Removal of orange-G and methyl violet dyes by adsorption onto bagasse fly ash-kinetic study and equilibrium isotherm analyses, *Dyes and Pigments*, **69**, 210-223.

Mehta S.K., Gaur J.P., (2001a), Characterization and optimization of Ni and Cu sorption from aqueous solution by Chlorella vulgaris, *Ecological Engineering*, **18**, 1-13.

Mehta S.K., Gaur J.P., (2001b), Concurrent sorption of Ni^{2+} and Cu^{2+} by Chlorella vulgaris from a binary metal solution, *Applied Microbiology and Biotechnology*, **55**, 379-382.

Mehta S.K., Gaur J.P., (2001c), Removal of Ni and Cu from single and binary metal solutions by free and immobilized *Chlorella vulgaris*, *European Journal of Protistology*, **37**, 261-271.

Mehta S.K., Singh A., Gaur J.P., (2002a), Kinetics of adsorption and uptake of Cu^{2+} by *Chlorella vulgaris*: influence of pH, temperature, culture age and cations, *Journal of Environmental Science and Health, Part A*, **37**, 399-414.

Mehta S.K., Tripathi B.N., Gaur J.P., (2002b), Enhanced sorption of Cu^{2+} and Ni^{2+} by acid-protected Chlorella vulgaris from single and binary metal solutions, *Journal of Applied Phycology*, **14**, 267-273.

Mgbemere H.E., Lawal G.I., Ekpe I.C., Chaudhary A.L., (2018), Synthesis of zeolite-A using kaolin samples from Darazo, Bauchi State and Ajebo, Ogun State in Nigeria, *Nigerian Journal of Technology*, **37**, 87-95.

Moshoeshoe M., Nadiye-Tabbiruka M.S., Obuseng V., (2017), A review of the chemistry, structure, properties and applications of zeolites, *American Journal of Materials Science*, **7**, 196-221.

Nethaji S., Sivasamy A., Mandal A.B., (2013), Adsorption isotherms, kinetics and mechanism for the adsorption of cationic and anionic dyes onto carbonaceous particles prepared from Juglans regia shell biomass, *International Journal of Environmental Science and Technology*, **10**, 231-242.

Ostroski I.C., Barros M.A.S.D., Silva E.A., Dantas J.-H., Arroyo P.A., Lima O.C.M., (2007), The removal of Fe(III) ions by adsorption onto zeolite columns, *Adsorption Science and Technology*, **25**, 757-768.

Passos F.A.C.M., Castro D.C., Ferreira K.K., Simões K.M.A., Bertolino L.C., Barbato C.N., Garrido F.M.S., Felix A.A.S., Silva F.A.N.G., (2017), *Synthesis and Characterization of Sodalite and Cancrinite from Kaolin*, In: *Characterization of Minerals, Metals, and Materials*, Ikhmayies S., Li B., Carpenter J.S., Li J., Hwang J.-Y., Monteiro S.N., Firrao D., Zhang M., Peng, Z., Escobedo-Diaz J.P., Bai C., Kalay Y.E., Goswami R., Kim J. (Eds.), vol 2017, The Minerals, Metals & Materials Series, Springer, Cham, 279-288.

Rad L.R., Momeni A., Ghazani B.F., Irani M., Mahmoudi M., Noghreh B., (2014), Removal of Ni^{2+} and Cd^{2+} ions from aqueous solutions using electrospun PVA/zeolite nanofibrous adsorbent, *Chemical Engineering Journal*, **256**, 119-127.

Ríos C.A.R., (2008), *Synthesis of zeolites from geological materials and industrial wastes for potential application in environmental problems*, PhD Thesis, University of Wolverhampton, Wolverhampton, United Kingdom.

Ríos C.A.R., Williams C.D., Roberts C.L., (2009), A comparative study of two methods for the synthesis of fly ash-based sodium and potassium type zeolites, *Fuel*, **88**, 1403-1416.

Ríos C.A.R., Williams C.D., Alarcón O.M.C., (2010), Synthesis of zeolite LTA from thermally treated kaolinite, *Revista Facultad de Ingeniería Universidad de Antioquia*, **53**, 30-41.

Robson H.E., (1998), *Verified Syntheses of Zeolitic Materials*, 1st Edition, Elsevier, Amsterdam.

Salih A.M., (2017), *The purification of industrial wastewater to remove heavy metals and investigation into the use of zeolite as a remediation tool*, PhD Thesis, University of Wolverhampton, Wolverhampton, United Kingdom.

Sari M.E.F., Suprapto S., Prasetyoko D., (2018), Direct synthesis of sodalite from kaolin: the influence of alkalinity, *Indonesian Journal of Chemistry*, **18**, 607-613.

Shirani Lapari S., Ramli Z., Triwahyono S., (2015), Effect of different templates on the synthesis of mesoporous sodalite, *Journal of Chemistry*, ID 272613, https://doi.org/10.1155/2015/272613.

Sprynskyy M., Buszewski B., Terzyk A.P., Namieśnik J., (2006), Study of the Selection Mechanism of Heavy Metal (Pb^{2+}, Cu^{2+}, Ni^{2+}, and Cd^{2+}) Adsorption on Clinoptilolite, *Journal of Colloid and Interface Science*, **304**, 21-28.

Taamneh Y., Sharadqah S., (2017), The removal of heavy metals from aqueous solution using natural Jordanian zeolite, *Applied Water Science*, **7**, 2021-2028.

Taylor A.A., Tsuji J.S., Garry M.R., McArdle M.E., Goodfellow Jr W.L., Adams W.J., Menzie C.A., (2020), Critical review of exposure and effects: implications for setting regulatory health criteria for ingested copper, *Environmental Management*, **65**, 131-159.

Thakur L.S., Parmar M., (2013), Adsorption of heavy metal (Cu^{2+}, Ni^{2+} and Zn^{2+}) from synthetic waste water by tea waste adsorbent, *International Journal of Chemical and Physical Sciences*, **2**, 6-19.

Tohdee K., Kaewsichan L., Ullah A., (2018), Enhancement of adsorption efficiency of heavy metal Cu(II) and Zn(II) onto cationic surfactant modified bentonite, *Journal of Environmental Chemical Engineering*, **6**, 2821-2828.

Van der Marel H.W., Beutelspacher H., (1976), *Atlas of Infrared Spectroscopy of Clay Minerals and Their Admixtures*, Elsevier, Amsterdam, 31-58.

Wang L., Chen Z., Yang J., Ma F., (2015), Pb(II) biosorption by compound bioflocculant: performance and mechanism, *Desalination and Water Treatment*, **53**, 421-429.

Widiastuti N., Wu H., Ang H.M., Zhang D., (2011), Removal of ammonium from greywater using natural zeolite, *Desalination*, **277**, 15-23.

Yao J., Zhang L., Wang H., (2008), Synthesis of nanocrystalline sodalite with organic additives, *Materials Letters*, **62**, 4028-4030.

Yurekli Y., (2016), Removal of heavy metals in wastewater by using zeolite nano-particles impregnated polysulfone membranes, *Journal of Hazardous Materials*, **309**, 53-64.